A quasi-analytical boundary condition for three-dimensional finite difference electromagnetic modeling

Salah Mehanee[1] and Michael Zhdanov

Consortium for Electromagnetic Modeling and Inversion, Department of Geology and Geophysics, University of Utah, Salt Lake City, Utah, USA

[1] Numerical modeling of the quasi-static electromagnetic (EM) field in the frequency domain in a three-dimensional (3-D) inhomogeneous medium is a very challenging problem in computational physics. We present a new approach to the finite difference (FD) solution of this problem. The FD discretization of the EM field equation is based on the balance method. To compute the boundary values of the anomalous electric field we solve for, we suggest using the fast and accurate quasi-analytical (QA) approximation, which is a special form of the extended Born approximation. We call this new condition a quasi-analytical boundary condition (QA BC). This approach helps to reduce the size of the modeling domain without losing the accuracy of calculation. As a result, a larger number of grid cells can be used to describe the anomalous conductivity distribution within the modeling domain. The developed numerical technique allows application of a very fine discretization to the area with anomalous conductivity only because there is no need to move the boundaries too far from the inhomogeneous region, as required by the traditional Dirichlet or Neumann conditions for anomalous field with boundary values equal to zero. Therefore this approach increases the efficiency of FD modeling of the EM field in a medium with complex structure. We apply the QA BC and the traditional FD (with large grid and zero BC) methods to complicated models with high resistivity contrast. The numerical modeling demonstrates that the QA BC results in 5 times matrix size reduction and 2–3 times decrease in computational time.   *INDEX TERMS:* 0644 Electromagnetics: Numerical methods; 0639 Electromagnetics: Nonlinear electromagnetics; 0925 Exploration Geophysics: Magnetic and electrical methods; *KEYWORDS:* finite difference, electromagnetic modeling, boundary conditions

1. Introduction

[2] In most geophysical applications of electromagnetic (EM) methods, it is necessary to model geoelectrical structures of quite arbitrary shape and size, with anomalous conductivity varying in an arbitrary manner. The most widely used approaches to EM forward modeling are finite difference (FD) and finite element (FE) methods to find numerical solutions to

Maxwell's equations written in differential form [*Weaver*, 1994; *Zhdanov et al.*, 1997; *Zhdanov*, 2002]. The FD method provides a simple but effective tool for numerically solving the EM forward modeling problem [*Weaver and Brewitt-Taylor*, 1978; *Zhdanov et al.*, 1982; *Zhdanov and Spichak*, 1992; *Weaver*, 1994; *Mackie et al.*, 1993, 1994; *Newman and Alumbaugh*, 1995; *Smith*, 1996; *Zhdanov et al.*, 1997; *Spichak*, 1999; *Haber et al.*, 2000]. One common technique of field discretization is based on a staggered-grid scheme [*Yee*, 1966; *Wang and Hohmann*, 1993; *Wang and Fang*, 2001; *Davydycheva et al.*, 2003], which is effective in solving the coupled first-order Maxwell's equations. Another approach to the discretization of the EM field equations is based on the balance method [*Zhdanov et al.*, 1982; *Samarsky*, 1984; *Zhdanov and Spichak*, 1989, 1992; *Zhdanov and Keller*,

[1]Now at Geophysics Department, Faculty of Science, Cairo University, Giza, Egypt.
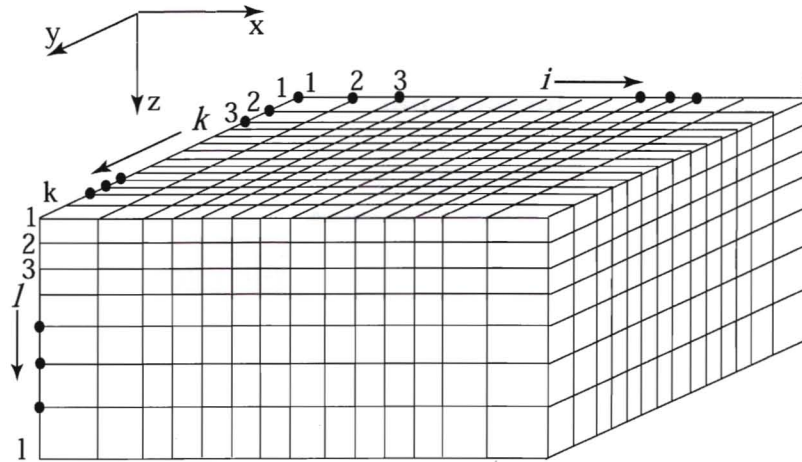
Figure 1. The model region is discretized into a number of prisms. The indices i, k, and l are used to number the grid point in the x, y, and z directions, respectively. Electrical conductivity (σ) is assumed to be constant within each elementary prism.

1994; *Spichak*, 1999; *Mehanee and Zhdanov*, 2001; *Zhdanov*, 2002; *Mehanee*, 2003]. This method involves integrating the original differential equations over each cell of the FD grid and discretizing the corresponding system of integral equations. The advantage of this approach is that it preserves the current balance in the volume and the corresponding charge conservation law.

[3] An important problem in FD implementation for the quasi-static EM field modeling in the frequency domain (which is typically used in geophysical applications) is selecting the proper boundary conditions for the field components. Usually, the boundaries of the modeling volume are set so far from the conductivity anomaly that it is possible to neglect the anomalous field there. In this case, the simplest Dirichlet boundary conditions of the first order can be implemented by choosing, e.g., zero boundary values when solving for the anomalous field. One can also use the simplest Neumann boundary conditions, which requires the normal gradient of the field to be zero at the boundary. Note, however, that application of the aforementioned simple conditions requires the size of the modeling region to exceed the size of the inhomogeneous region many times over, in order to be able to neglect the effect of the anomalous fields at the boundaries. To overcome this limitation, one can use asymptotic boundary conditions, developed for two-dimensional (2-D) models by *Weaver and Brewitt-Taylor* [1978], and extended to three-dimensional (3-D) models by *Zhdanov et al.* [1982] and *Berdichevsky and Zhdanov* [1984]. These conditions are based on the analysis of the asymptotic behavior of the EM field far away from

the geoelectrical anomalies. We should notice, however, that the majority of papers on 3-D quasi-static EM field modeling still use a simple Dirichlet boundary condition of the first order with zero values at the boundaries [e.g., *Newman and Alumbaugh*, 1995; *Fomenko and Mogi*, 2002].

[4] We should mention also the Perfect Matched Layer (PML) absorbing boundary condition (ABC) [*Berenger*, 1994]. The PML ABC was introduced mainly for FD time domain EM modeling. It is used for terminating the computation domain in order to absorb the outgoing EM waves [*Turkel and Yefet*, 1998]. However, in the case of the quasi-static EM field, which is the subject of our research, it is difficult to use the model of EM waves and their reflection from the boundaries because the field propagates according to the diffusion law. That is why the original PML ABC, developed for the FD time domain EM field, has found little application in modeling the quasi-static EM field used in geophysical applications.

[5] In this paper, we propose a different approach to the solution of this problem. To compute the boundary values of the anomalous electric field, we suggest using the fast and accurate quasi-analytical (QA) approximation [*Zhdanov et al.*, 2000], which is a special form of the extended Born approximation [*Habashy et al.*, 1993]. These precomputed values are then used as boundary conditions for the FD modeling based on the balance method. We will demonstrate that this approach allows significant reduction in the size of the FD grid in both air and earth without losing the accuracy of the calculations. As a result one can apply a very fine discretization to the area with anomalous conductivity because there is no
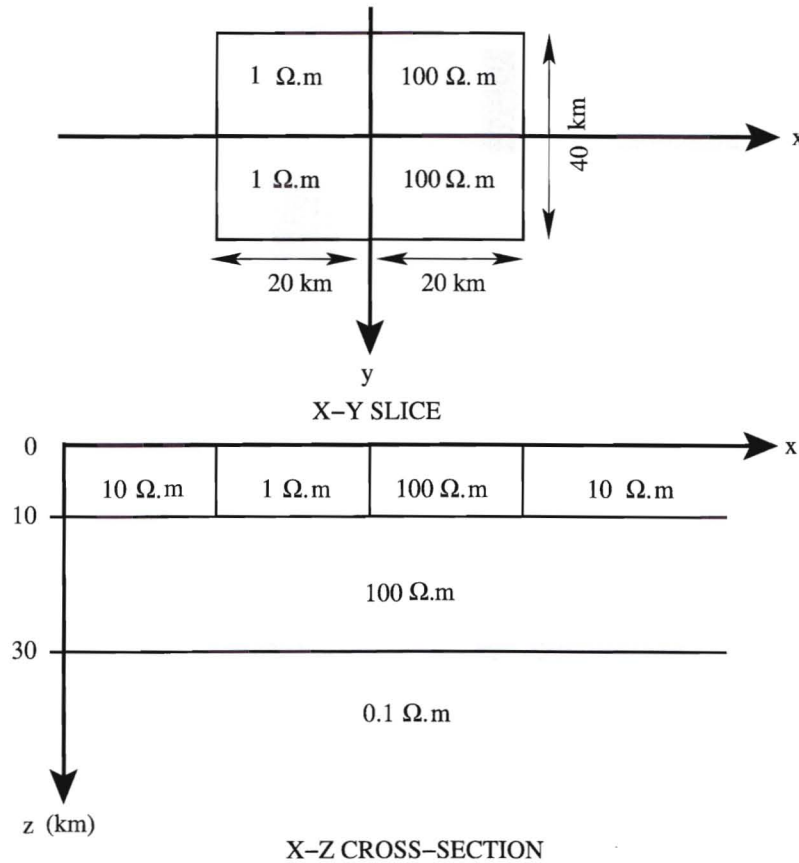
Figure 2.   Model 1: COMMEMI model 3d2 [after *Zhdanov et al.*, 1997].

need to move the boundaries too far from the inhomogeneous region.

2. Finite Difference Approximation of the Anomalous Electric Field Using the Balance Method

[6] Consider a 3-D geoelectrical model with a background conductivity σ_b and a local inhomogeneity D with an arbitrarily varying conductivity $\sigma = \sigma_b + \Delta\sigma$, where $\Delta\sigma$ is the anomalous conductivity. We will confine ourselves to consideration of nonmagnetic media and, hence, assume that $\mu = \mu_0 = 4\pi \times 10^{-7} H/m$, where μ_0 is the free-space magnetic permeability. The model is excited by an electromagnetic field generated by an arbitrary source with extraneous current distribution $\mathbf{j}^e$. This field is time harmonic as $e^{-i\omega t}$, where ω is the frequency (Hz).

[7] In geophysical applications, it is important to incorporate different types of excitation sources in electromagnetic modeling. The most convenient way to do that is to separate the total electric (**E**) and magnetic (**H**) fields into background (normal) and anomalous parts,
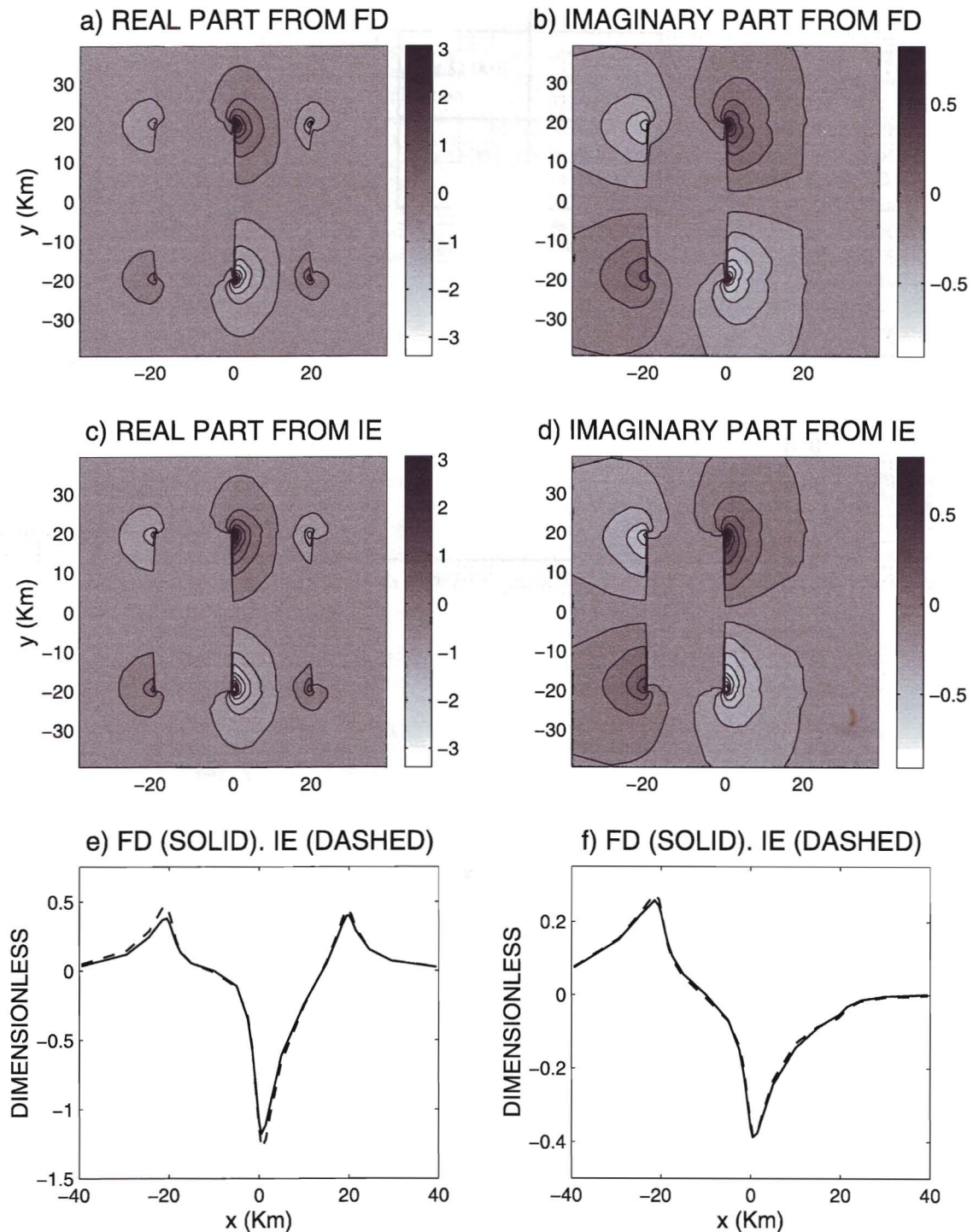
$$\mathbf{E} = \mathbf{E}^b + \mathbf{E}^a, \ \mathbf{H} = \mathbf{H}^b + \mathbf{H}^a, \qquad (1)$$

where the background (normal) fields ($\mathbf{E}^b$, $\mathbf{H}^b$) are generated by a given source for a model with a layered-earth (normal) conductivity distribution (σ_b), and the anomalous fields ($\mathbf{E}^a$, $\mathbf{H}^a$) are produced by the anomalous conductivity distribution ($\Delta\sigma = \sigma - \sigma_b$). Note also that this approach usually provides more stable and accurate numerical solution than the total EM field formulation [*Fomenko and Mogi*, 2002]. The second-order partial differential equation for the anomalous electric field $\mathbf{E}^a$ can be written as [*Zhdanov*, 2002]:

$$\nabla \times (\nabla \times \mathbf{E}^a) - i\omega\mu_0\sigma\mathbf{E}^a = i\omega\mu\Delta\sigma\mathbf{E}^b. \qquad (2)$$

Using the known vector identity, we can re-write equation (2) as:

$$\nabla(\nabla \cdot \mathbf{E}^a) - \nabla^2\mathbf{E}^a = i\omega\mu_0\sigma\mathbf{E}^a + i\omega\mu\Delta\sigma\mathbf{E}^b. \qquad (3)$$

a) REAL PART FROM FD

b) IMAGINARY PART FROM FD

c) REAL PART FROM IE

d) IMAGINARY PART FROM IE

e) FD (SOLID). IE (DASHED)

f) FD (SOLID). IE (DASHED)

Figure 3. Model 1. Electric field E_x component at Earth's surface obtained by finite difference (FD) and integral equation (IE) modeling: (a and b) real and imaginary parts obtained from FD; (c and d) real and imaginary parts obtained from IE; (e and f) profiles in the x direction at y = −21.5 km of the real and imaginary parts obtained from FD (solid line) and IE (dashed line). The electric field results shown are total electric field normalized by the corresponding incident normal (background) field computed at Earth's surface.
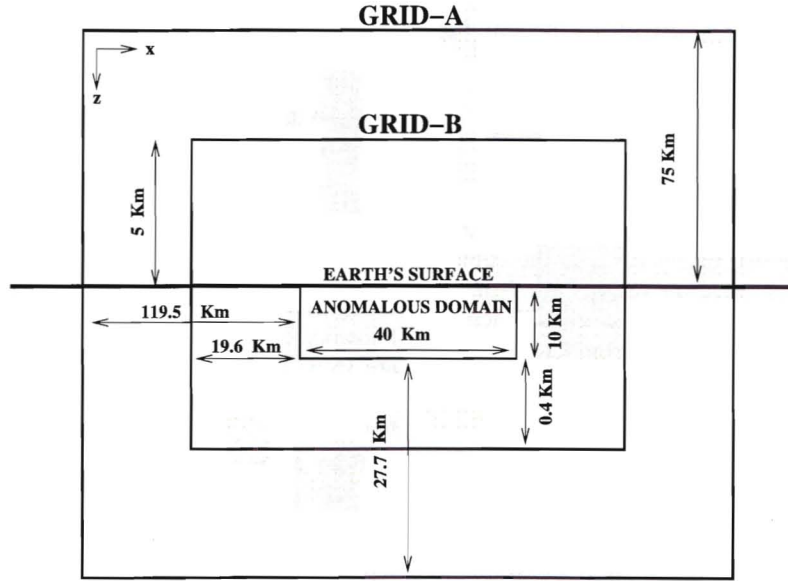
Figure 4. This figure shows an x-z sketch (at y = 0, Figure 2) of both the untruncated (GRID-A) and truncated (GRID-B) FD grids used in model 1 forward modelings in order to verify the quasi-analytical (QA)-based boundary conditions (BC). GRID-A and GRID-B, respectively, utilize the zero and QA-based BC. The detailed model description is shown in Figure 2. The y-z section has distances identical to those shown above.

The anomalous magnetic field $\mathbf{H}^a$ is expressed in terms of $\mathbf{E}^a$ as:

$$\mathbf{H}^a = \frac{1}{i\omega\mu_0}\nabla \times \mathbf{E}^a. \qquad (4)$$

By taking the divergence of the first Maxwell's equation for the anomalous electric field, we obtain:

$$-\nabla(\mathbf{E}^a \cdot \nabla \ln \sigma) - \nabla^2 \mathbf{E}^a - i\omega\mu_0\sigma\mathbf{E}^a = i\omega\mu_0\Delta\sigma\mathbf{E}^b$$
$$+ \nabla\left(\mathbf{E}^b \cdot \nabla \ln \frac{\sigma}{\sigma_b}\right). \qquad (5)$$

Let us assume that the region of modeling, V, is bounded by a surface ∂V. We discretize the model region into a number of prisms as shown in Figure 1. A Cartesian coordinate system is defined with the z axis directed downward and the x axis directed to the right. The indices $i, k,$ and l are used to number the grid point in the $x, y,$ and z directions, respectively. We denote this grid by $\sum$:

$$\sum = \left\{ (x_i, y_k, z_l) \quad \begin{array}{l} x_{i+1} = x_i + \Delta x_i, i = 1, 2, .., I-1 \\ y_{k+1} = y_k + \Delta y_k, k = 1, 2, .., K-1 \\ z_{l+1} = z_l + \Delta z_l, l = 1, 2, .., L-1 \end{array} \right\}.$$

The electrical conductivity is assumed to be constant within each elementary prism. In the balance method

[Zhdanov, 2002], the conductivity is discretized on a rectangular, uneven 3-D dual grid $\widetilde{\sum}$ consisting of nodal points located at the centers of each cell of the original mesh $\sum$:

$$\widetilde{\sum} = \left\{ (x_{i+\frac{1}{2}}, y_{k+\frac{1}{2}}, z_{l+\frac{1}{2}}) \quad \begin{array}{l} x_{i+\frac{1}{2}} = x_i + \Delta x_i/2, \ i = 1, .., I-1 \\ y_{k+\frac{1}{2}} = y_k + \Delta y_k/2, \ k = 1, .., K-1 \\ z_{l+\frac{1}{2}} = z_l + \Delta z_l/2, \ l = 1, .., L-1 \end{array} \right\}.$$

We introduce the discretized vector function $\mathbf{E}^a_{i,k,l} = \mathbf{E}^a(x_i, y_k, z_l)$ on the grid $\sum$, and the discretized scalar function $\sigma_{i+\frac{1}{2},k+\frac{1}{2},l+\frac{1}{2}} = \sigma(x_{i+\frac{1}{2}}, y_{k+\frac{1}{2}}, z_{l+\frac{1}{2}})$ on the dual grid $\widetilde{\sum}$.

[8] In constructing a proper FD scheme for solution of this problem by the balance method, we do not use equation (5), but rather an integral identity obtained by integrating equation (5) over an elementary cell V_{ikl} of the dual mesh $\widetilde{\sum}$ based on the vector statements of the Gauss theorem [Zhdanov, 1988]:

$$-\int\int_{S_{ikl}} (\mathbf{E}^a \cdot \nabla \ln \sigma)\mathbf{n}ds - \int\int_{S_{ikl}} (\mathbf{n} \cdot \nabla)\mathbf{E}^a ds$$
$$- i\omega\mu_0 \int\int\int_{V_{ikl}} \sigma\mathbf{E}^a dv = \int\int_{S_{ikl}} \left(\mathbf{E}^b \cdot \nabla \ln \frac{\sigma}{\sigma_b}\right)\mathbf{n}ds$$
$$+ i\omega\mu_0 \int\int\int_{V_{ikl}} \Delta\sigma\mathbf{E}^b dv, \qquad (6)$$

where S_{ikl} is the rectangular boundary of the cell V_{ikl}, formed by six sides $S_{i\pm\frac{1}{2},k,l}$, $S_{i,k\pm\frac{1}{2},l}$, and $S_{i,k,l\pm\frac{1}{2}}$:

$$S_{ikl} = S_{i+\frac{1}{2},k,l} \cup S_{i-\frac{1}{2},k,l} \cup S_{i,k+\frac{1}{2},l} \cup S_{i,k-\frac{1}{2},l} \cup S_{i,k,l+\frac{1}{2}} \cup S_{i,k,l-\frac{1}{2}},$$

and $\mathbf{n}$ is a unit vector normal to S_{ikl} and directed out of the volume. We can approximately evaluate the volume and surface integrals in equation (6) in terms of the discretized electric field vector $\mathbf{E}^a_{i,k,l}$ and scalar functions $\sigma_{i+\frac{1}{2},k+\frac{1}{2},l+\frac{1}{2}}$. In particular, we can use a simple relationship to approximate the following integral as:

$$i\omega\mu_0 \int\int\int_{V_{ikl}} \sigma \mathbf{E}^a \, dv \approx i\omega\mu_0 \mathbf{E}^a_{i,k,l} \int\int\int_{V_{ikl}} \sigma \, dv.$$

The surface integrals are computed using a simple difference form. For example:

$$\int\int_{S_{ikl}} (\mathbf{n} \cdot \nabla)\mathbf{E}^a ds = \int\int_{S_{ikl}} \frac{\partial \mathbf{E}^a}{\partial n} ds, \quad (7)$$

and the derivative $\partial \mathbf{E}^a / \partial n$ is approximated as:

$$\left.\frac{\partial \mathbf{E}^a}{\partial x}\right|_{S_{i+\frac{1}{2},k,l}} \approx \frac{\mathbf{E}^a_{i+1,k,l} - \mathbf{E}^a_{i,k,l}}{\Delta x_i}. \quad (8)$$

The surface integral

$$\int\int_{S_{ikl}} (\mathbf{E}^a \cdot \nabla \ln \sigma)\mathbf{n} ds, \quad (9)$$

can be evaluated in a similar way. The derivatives of $\ln \sigma$ are calculated using a three-point FD scheme [*Zhdanov and Spichak*, 1992; *Kincaid and Cheney*, 1996]. The values of the electric field on the sides $S_{i\pm\frac{1}{2}}$, $S_{k\pm\frac{1}{2}}$, and $S_{l\pm\frac{1}{2}}$ of the cell V_{ikl} are approximated by the corresponding average field values computed at the nodes of the grid $\sum$:

$$\mathbf{E}^a\big|_{S_{i\pm\frac{1}{2}}} = \frac{1}{2}\left(\mathbf{E}^a_{i\pm1,k,l} + \mathbf{E}^a_{i,k,l}\right),$$

$$\mathbf{E}^a\big|_{S_{k\pm\frac{1}{2}}} = \frac{1}{2}\left(\mathbf{E}^a_{i,k\pm1,l} + \mathbf{E}^a_{i,k,l}\right),$$

$$\mathbf{E}^a\big|_{S_{l\pm\frac{1}{2}}} = \frac{1}{2}\left(\mathbf{E}^a_{i,k,l\pm1} + \mathbf{E}^a_{i,k,l}\right). \quad (10)$$

The surface integrals are calculated using the rectangular rule [*Zhdanov*, 2002]. The resulting stencil for the electric field $\mathbf{E}^a$ has seven points located at the nodal points of the grid $\sum$.

[9] The resulting system of linear algebraic equations and the accompanying boundary conditions can be expressed in matrix notation as:

$$\left(\widehat{\mathbf{D}} + i\omega\mu_0\widehat{\sigma}\right)\mathbf{e}^a = i\omega\mu_0\widehat{\Delta\sigma}\mathbf{e}^b + \mathbf{f}\left(\widehat{\Delta\sigma}, \mathbf{e}^b\right) + \mathbf{b}, \quad (11)$$

where $\mathbf{e}^a$ and $\mathbf{e}^b$ are column vectors of length $3N$ of the unknown values of the anomalous electric field and known values of the background electric field; $\widehat{\sigma}$ and $\widehat{\Delta\sigma}$ are $3N \times 3N$ diagonal matrices of the integrated total and anomalous conductivities over the grid $\sum$; $\widehat{\mathbf{D}}$ is a $3N \times 3N$ matrix of coefficients which is independent of frequency ω; $\mathbf{f}(\widehat{\Delta\sigma}, \mathbf{e}^b)$ is a column vector of length $3N$ depending on the anomalous conductivities and the background field; and $\mathbf{b}$ is a column vector of length $3N$ determined by the boundary value conditions.

[10] The structure of the matrix $\widehat{\mathbf{D}}$ essentially depends on the method used to order the vector $\mathbf{e}^a$ and on the choice of boundary conditions. In the simplest case, the nodes of the mesh are numbered consecutively along the horizontal and vertical directions. Note that for the given numbering of the nodes, $n = 1, 2, 3.., N, (N = IKL)$ one can establish a simple one-to-one relationship between the index n and the triple number (i, k, l):

$$n = i + (k - 1)I + (l - 1)IK. \quad (12)$$

[11] In this case, matrix $\widehat{\mathbf{D}}$ has a septa-block-diagonal structure:

$$\widehat{\mathbf{D}} = \begin{bmatrix} \widehat{\mathbf{d}}_1^{(0)} & \widehat{\mathbf{d}}_1^{(+x)} & 0.. & \widehat{\mathbf{d}}_1^{(+y)} & 0. & \widehat{\mathbf{d}}_1^{(+z)} & 0.. & .0 \\ \widehat{\mathbf{d}}_2^{(-x)} & \widehat{\mathbf{d}}_2^{(0)} & \widehat{\mathbf{d}}_2^{(+x)} & 0.. & \widehat{\mathbf{d}}_2^{(+y)} & 0.. & \widehat{\mathbf{d}}_2^{(+z)} & .0 \\ 0 & \widehat{\mathbf{d}}_3^{(-x)} & \widehat{\mathbf{d}}_3^{(0)} & \widehat{\mathbf{d}}_3^{(+x)} & .. & .. & .. & .\widehat{\mathbf{d}}_{N-IK}^{(+y)} \\ \widehat{\mathbf{d}}_{I+1}^{(-y)} & 0. & .. & .. & .. & .. & .. & .0 \\ 0. & .. & .. & .. & .. & .. & .. & .\widehat{\mathbf{d}}_{N-I}^{(+y)} \\ \widehat{\mathbf{d}}_{IK+1}^{(-z)} & 0.. & .. & .. & .. & .. & .. & .0 \\ 0. & .. & .. & .. & .. & .. & .. & .\widehat{\mathbf{d}}_{N-1}^{(+x)} \\ .0 & .0 & \widehat{\mathbf{d}}_N^{(-z)} & .0 & \widehat{\mathbf{d}}_N^{(-y)} & .0 & \widehat{\mathbf{d}}_N^{(-x)} & .\widehat{\mathbf{d}}_N^{(0)} \end{bmatrix},$$

and the vector $\mathbf{e}^a$ has the structure:

$$\mathbf{e}^a = \begin{bmatrix} E_{x,1} & E_{y,1} & E_{z,1} & E_{x,2} & E_{y,2} & E_{z,2} & .. & .. & .. & E_{x,N} & E_{y,N} & E_{z,N} \end{bmatrix}^T.$$

The preconditioned generalized minimal residual (GMRES) method [*Saad and Schultz*, 1986; *Zhdanov*, 2002], from the Portable, Extensible Toolkit for

Scientific Computation (PETSC) [*Balay et al.*, 1997, 2000] (see also http://www.mcs.anl.gov/petsc), is used here to solve the system (11) (see Appendix A).

3. Boundary Value Conditions Based on the Quasi-Analytical Approximation

[12] In this section we discuss a new technique for determining the boundary conditions of the EM field for 3-D FD modeling. The traditional statements of boundary value problems are based on applying Dirichlet boundary value conditions of the first, second, or third order, formed by means of linear combinations of the field itself and its derivative normal to the boundary. Dirichlet boundary conditions of the first order fix the values of the field at the boundary. Dirichlet boundary conditions of the second order, or Neumann boundary conditions, fix the field normal gradient value to the boundary; and Dirichlet boundary conditions of the third order, or Cauchy boundary conditions, fix both value and the normal gradient of the field at the boundary [*Morse and Feshbach*, 1953].

[13] Usually, the boundaries of the modeling domain are set very far from the anomalous domain such that it is possible to neglect the anomalous field there. In this case, the simplest Dirichlet boundary conditions of the first order can be implemented by setting the anomalous field to zero at the boundaries [*Fomenko and Mogi*, 2002]. Another approach is based on the simplest Neumann boundary conditions which set the normal gradient of the field to zero at the boundaries.

[14] In a general case, the appropriate boundary distance depends on the size of the anomalous domain, the background conductivity, the frequency, and the type of source. In the present paper we solve the FD equations for the anomalous field, which reduces the effect of the type of source on the boundary distance selection. The most significant effect is attributed to the wavelength λ_b (or skin depth δ_b) of the EM field in the background medium, where $\delta_b = \lambda_b/2\pi$ and $\lambda_b = 2\pi/(\omega\mu_0\sigma_b/2)^{1/2}$. In practical computations, one can use zero boundary conditions if the distance, d_b, from the anomalous domain to the boundary of the modeling grid is at least three to five skin depths. Note that the simple boundary conditions outlined above could require a modeling grid that is too large if we consider a low frequency (below 1 Hz) and a resistive background (100 Ohm-m or more), which is a typical case for many geophysical applications. Otherwise the anomalous field can be inaccurate if it is not actually equal to zero at the boundaries.

[15] To overcome this problem we suggest using, as a Dirichlet boundary condition, the values of the anomalous electric field computed by the quasi-analytical (QA) approximation [*Zhdanov et al.*, 2000]. The QA approximation represents a special form of the extended Born approximation introduced by *Habashy et al.* [1993]. In the framework of the QA approximation, the anomalous electric field is computed at the boundaries of the modeling domain using a simple integration [*Zhdanov et al.*, 2000] as:

$$\mathbf{E}_{QA}^a(\mathbf{r}_j) = \mathbf{E}(\mathbf{r}_j) - \mathbf{E}^b(\mathbf{r}_j)$$
$$= \int\int\int_D \widehat{\mathbf{G}}_E(\mathbf{r}_j \mid \mathbf{r}) \cdot \left[\frac{\Delta\sigma(\mathbf{r})}{1 - g(\mathbf{r})} \mathbf{E}^b(\mathbf{r})\right] dv, \tag{13}$$

where $\widehat{\mathbf{G}}_E(\mathbf{r}_j|\mathbf{r})$ is the electric Green's tensors defined for an unbounded conductive medium with a background conductivity σ_b. The numerical methods for computing the Green's tensors are very well developed. The interested reader may find more information about these methods in the work of *Anderson* [1979] and *Wannamaker et al.* [1984]. The function $g(\mathbf{r})$ is the normalized dot product of the Born approximation $\mathbf{E}^B$ and the background field $\mathbf{E}^b$,

$$g(\mathbf{r}) = \frac{\mathbf{E}^B(\mathbf{r}) \cdot \mathbf{E}^{b*}(\mathbf{r})}{\mathbf{E}^b(\mathbf{r}) \cdot \mathbf{E}^{b*}(\mathbf{r})}, \text{ assuming } \mathbf{E}^b(\mathbf{r}) \cdot \mathbf{E}^{b*}(\mathbf{r}) \neq 0, \tag{14}$$

where the asterisk means complex conjugate vector. Note that the condition given by equation (14) can be relaxed. In fact,

$$\frac{1}{1 - g(\mathbf{r})} = \frac{\mathbf{E}^b(\mathbf{r}) \cdot \mathbf{E}^{b*}(\mathbf{r})}{\mathbf{E}^b(\mathbf{r}) \cdot \mathbf{E}^{b*}(\mathbf{r}) - \mathbf{E}^B(\mathbf{r}) \cdot \mathbf{E}^b(\mathbf{r})},$$

which causes no problem unless

$$\mathbf{E}^b(\mathbf{r}) \cdot \mathbf{E}^{b*}(\mathbf{r}) = \mathbf{E}^B(\mathbf{r}) \cdot \mathbf{E}^{b*}(\mathbf{r}).$$

The values $\mathbf{E}_{QA}^a$ are used subsequently as boundary conditions for the FD modeling scheme.

Figure 5. Model 1. Electric field E_x component at Earth's surface obtained by FD modeling using different grid sizes and boundary conditions: (a and b) real and imaginary parts obtained from untruncated grid supplemented with zero BC (shown in solid line in Figures 5g and 5h; (c and d) real and imaginary parts obtained from truncated grid supplemented with QA BC (shown in dashed line in Figures 5g and 5h); (e and f) real and imaginary parts obtained from truncated grid supplemented with zero BC (shown in dash-dot line Figures 5g and 5h); (g and h) profiles in the x direction at y = −21.5 km of the real and imaginary parts, respectively. The electric field results shown are total electric field normalized by the corresponding incident normal (background) field computed at Earth's surface.
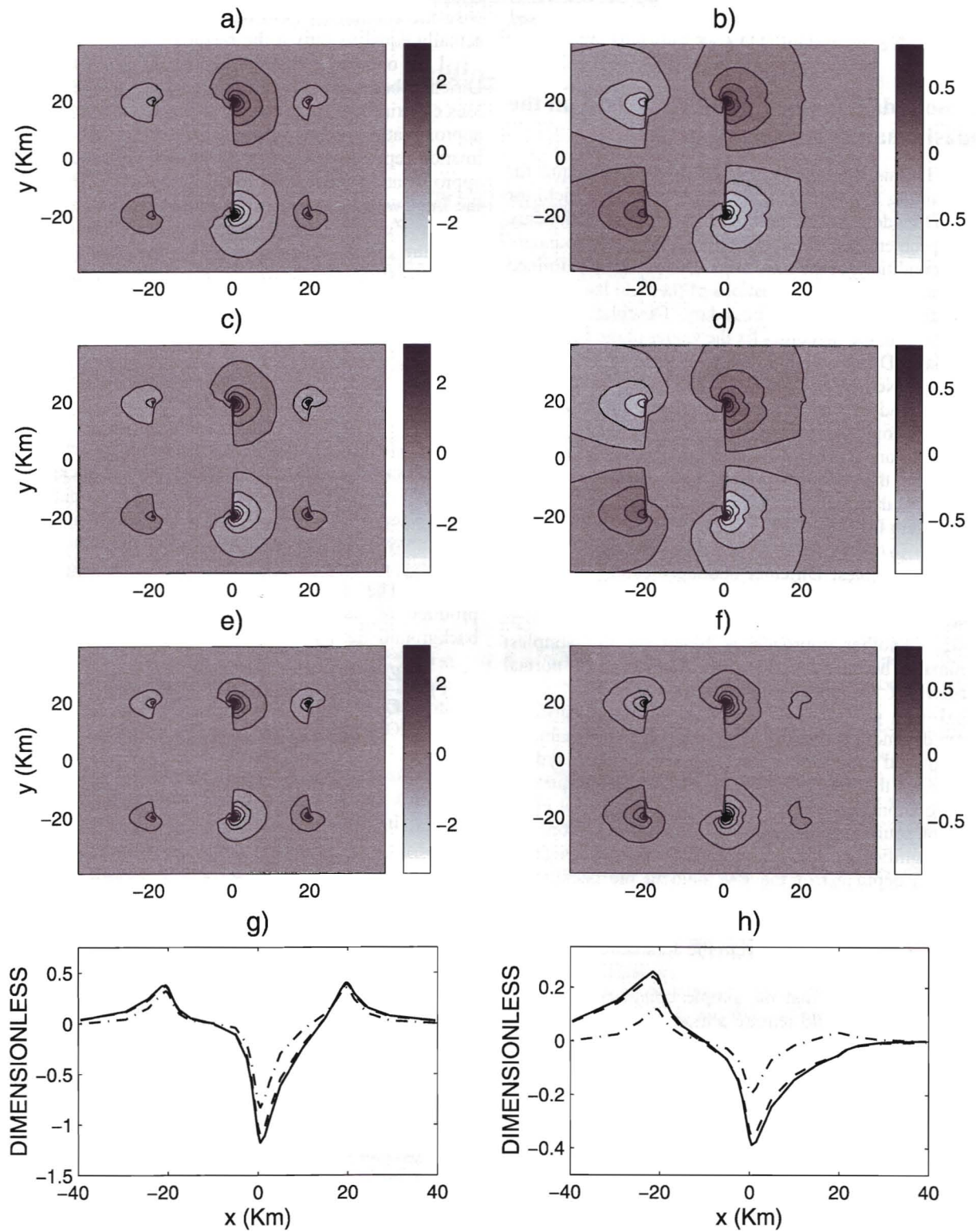
Figure 5

[16] In order to numerically evaluate (13), the anomalous domain (D) is discretized into N cells, each having a constant anomalous conductivity $\Delta\sigma$ and electric field values. The anomalous electric field is expressed using the full integral equation as:

$$\mathbf{E}^a(\mathbf{r}_j) = \mathbf{G}_E\left[\Delta\sigma(\mathbf{r})\left(\mathbf{E}^b(\mathbf{r}) + \mathbf{E}^a(\mathbf{r})\right)\right], \qquad (15)$$

which can be written in a discrete form [*Hursan and Zhdanov*, 2002] as:

$$\mathbf{e}^a = \widehat{\mathbf{G}}_D\widehat{\mathbf{S}}^a\left(\mathbf{e}^a + \mathbf{e}^b\right), \qquad (16)$$

where $\widehat{\mathbf{G}}_D$ is a $3N \times 3N$ matrix containing the electric Green's tensor integrals

$$\widehat{\mathbf{G}}_D = \begin{bmatrix} \Gamma_{xx}^{11} & \cdots & \Gamma_{xx}^{1N} & \Gamma_{xy}^{11} & \cdots & \Gamma_{xy}^{1N} & \Gamma_{xz}^{11} & \cdots & \Gamma_{xz}^{1N} \\ & & & & \vdots & & & & \\ \Gamma_{xx}^{N1} & \cdots & \Gamma_{xx}^{NN} & \Gamma_{xy}^{N1} & \cdots & \Gamma_{xy}^{NN} & \Gamma_{xz}^{N1} & \cdots & \Gamma_{xz}^{NN} \\ \Gamma_{yx}^{11} & \cdots & \Gamma_{yx}^{1N} & \Gamma_{yy}^{11} & \cdots & \Gamma_{yy}^{1N} & \Gamma_{yz}^{11} & \cdots & \Gamma_{yz}^{1N} \\ & & & & \vdots & & & & \\ \Gamma_{yx}^{N1} & \cdots & \Gamma_{yx}^{NN} & \Gamma_{yy}^{N1} & \cdots & \Gamma_{yy}^{NN} & \Gamma_{yz}^{N1} & \cdots & \Gamma_{yz}^{NN} \\ \Gamma_{zx}^{11} & \cdots & \Gamma_{zx}^{1N} & \Gamma_{zy}^{11} & \cdots & \Gamma_{zy}^{1N} & \Gamma_{zz}^{11} & \cdots & \Gamma_{zz}^{1N} \\ & & & & \vdots & & & & \\ \Gamma_{zx}^{N1} & \cdots & \Gamma_{zx}^{NN} & \Gamma_{zy}^{N1} & \cdots & \Gamma_{zy}^{NN} & \Gamma_{zz}^{N1} & \cdots & \Gamma_{zz}^{NN} \end{bmatrix},$$

$$\Gamma_{\alpha\beta}^{jk} = \int\int\int_{D_k} G_{\alpha\beta}^E(\mathbf{r}_j \mid \mathbf{r}_k)dv, \quad \alpha,\beta = x,y,z,$$

$\mathbf{e}^b$ and $\mathbf{e}^a$ are $3N \times 1$ vector columns of the background and anomalous fields,

$$\mathbf{e}^b = \left[E_{x,1}^b, ..E_{x,N}^b, E_{y,1}^b, ..E_{y,N}^b, E_{z,1}^b, ..E_{z,N}^b\right]^T,$$

$$\mathbf{e}^a = \left[E_{x,1}^a, ..E_{x,N}^a, E_{y,1}^a, ..E_{y,N}^a, E_{z,1}^a, ..E_{z,N}^a\right]^T,$$

and $\widehat{\mathbf{S}}^a$ is a $3N \times 3N$ diagonal matrix with the anomalous conductivities,

$$\widehat{\mathbf{S}}^a = diag([\Delta\widetilde{\sigma}_1, .., \Delta\widetilde{\sigma}_N, \Delta\widetilde{\sigma}_1, .., \Delta\widetilde{\sigma}_N, \Delta\widetilde{\sigma}_1, .., \Delta\widetilde{\sigma}_N]).$$

We can also define the matrix with background conductivity values inside each cell as:

$$\widehat{\mathbf{S}}^b = diag\left([\widetilde{\sigma}_1^b, .., \widetilde{\sigma}_N^b, \widetilde{\sigma}_1^b, .., \widetilde{\sigma}_N^b, \widetilde{\sigma}_1^b, .., \widetilde{\sigma}_N^b]\right).$$

Equation (16) is then solved iteratively [*Saad and Schultz*, 1986; *Golub and Van Loan*, 1996; *Hursan and Zhdanov*, 2002; *Zhdanov*, 2002].

[17] However, *Zhdanov* [2002] showed that the quasi-analytical approximation of the anomalous electric field (13) at the observation points can be written in a discrete form as:

$$\mathbf{e}_{QA}^a = \widehat{\mathbf{G}}_E\widehat{\mathbf{e}}_D^b[\mathbf{diag}(\mathbf{I} - \mathbf{g}(\sigma))]^{-1}\,\sigma,$$

where $\mathbf{I}$ is an $N \times 1$ column vector whose elements are all unity, and $\mathbf{g}(\sigma)$ is an $N \times 1$ column vector which represents the function $g(\mathbf{r})$ at the center of each cell of the anomalous domain, and is defined as:

$$\mathbf{g}(\sigma) = \left[\frac{\mathbf{E}^{b,1*} \cdot \mathbf{E}^{B,1}}{\mathbf{E}^{b,1*} \cdot \mathbf{E}^{b,1}}, \frac{\mathbf{E}^{b,2*} \cdot \mathbf{E}^{B,2}}{\mathbf{E}^{b,2*} \cdot \mathbf{E}^{b,2}}, \ldots, \frac{\mathbf{E}^{b,N*} \cdot \mathbf{E}^{B,N}}{\mathbf{E}^{b,N*} \cdot \mathbf{E}^{b,N}}\right]^T,$$

where $\mathbf{E}^{B,j}$ and $\mathbf{E}^{b,j}$ ($j = 1, 2, ..N$), respectively, denote the Born approximation and the background electric field in each cell within the anomalous domain. σ is an $N \times 1$ column vector whose elements are the anomalous conductivity of the cells of the anomalous domain.

[18] The vector $\mathbf{g}(\sigma)$ can be expressed in matrix multiplication [*Zhdanov*, 2002] as:

$$\mathbf{g}(\sigma) = \left(\widehat{\mathbf{e}}_D^b\widehat{\mathbf{e}}_D^{b*}\right)^{-1}\widehat{\mathbf{e}}_D^{b*}\mathbf{e}_D^B, \qquad (17)$$

where the Born approximation vector inside the anomalous domain, $\mathbf{e}_D^B$, can be expressed as

$$\mathbf{e}_D^B = \widehat{\mathbf{G}}_D\widehat{\mathbf{e}}_D^b\sigma. \qquad (18)$$

Substituting (18) into (17), we obtain

$$\mathbf{g}(\sigma) = \left(\widehat{\mathbf{e}}_D^b\widehat{\mathbf{e}}_D^{b*}\right)^{-1}\widehat{\mathbf{e}}_D^{b*}\mathbf{e}_D^B = \left(\widehat{\mathbf{e}}_D^b\widehat{\mathbf{e}}_D^{b*}\right)^{-1}\widehat{\mathbf{e}}_D^{b*}\widehat{\mathbf{G}}_D\widehat{\mathbf{e}}_D^b\sigma = \widehat{\mathbf{C}}\sigma,$$

where $\widehat{\mathbf{C}}$ is a matrix independent of the anomalous conductivity distribution, and is defined as:

$$\widehat{\mathbf{C}} = \left(\widehat{\mathbf{e}}_D^b\widehat{\mathbf{e}}_D^{b*}\right)^{-1}\widehat{\mathbf{e}}_D^{b*}\widehat{\mathbf{G}}_D\widehat{\mathbf{e}}_D^b.$$

Thus we can represent equation (13) for the anomalous electric field as:

$$\mathbf{e}_{QA}^a = \widehat{\mathbf{A}}_E\left[\mathbf{diag}\left(\mathbf{I} - \widehat{\mathbf{C}}\sigma\right)\right]^{-1}\sigma = \widehat{\mathbf{A}}_E\widehat{\mathbf{B}}(\sigma)\,\sigma,$$

where $\widehat{\mathbf{A}}_E = \widehat{\mathbf{G}}_E\widehat{\mathbf{e}}_D^b$ and $\widehat{\mathbf{B}}(\sigma) = \left[\mathbf{diag}\left(\mathbf{I} - \widehat{\mathbf{C}}\sigma\right)\right]^{-1}$.

[19] These QA values are precomputed at the nodal points of the boundaries of the truncated FD domain, which are then multiplied by the corresponding FD coefficients. These multiplication results are represented as the term $\mathbf{b}$ of the right-hand side of equation (11). Using the QA approximation (or even QA series [*Zhdanov et al.*,
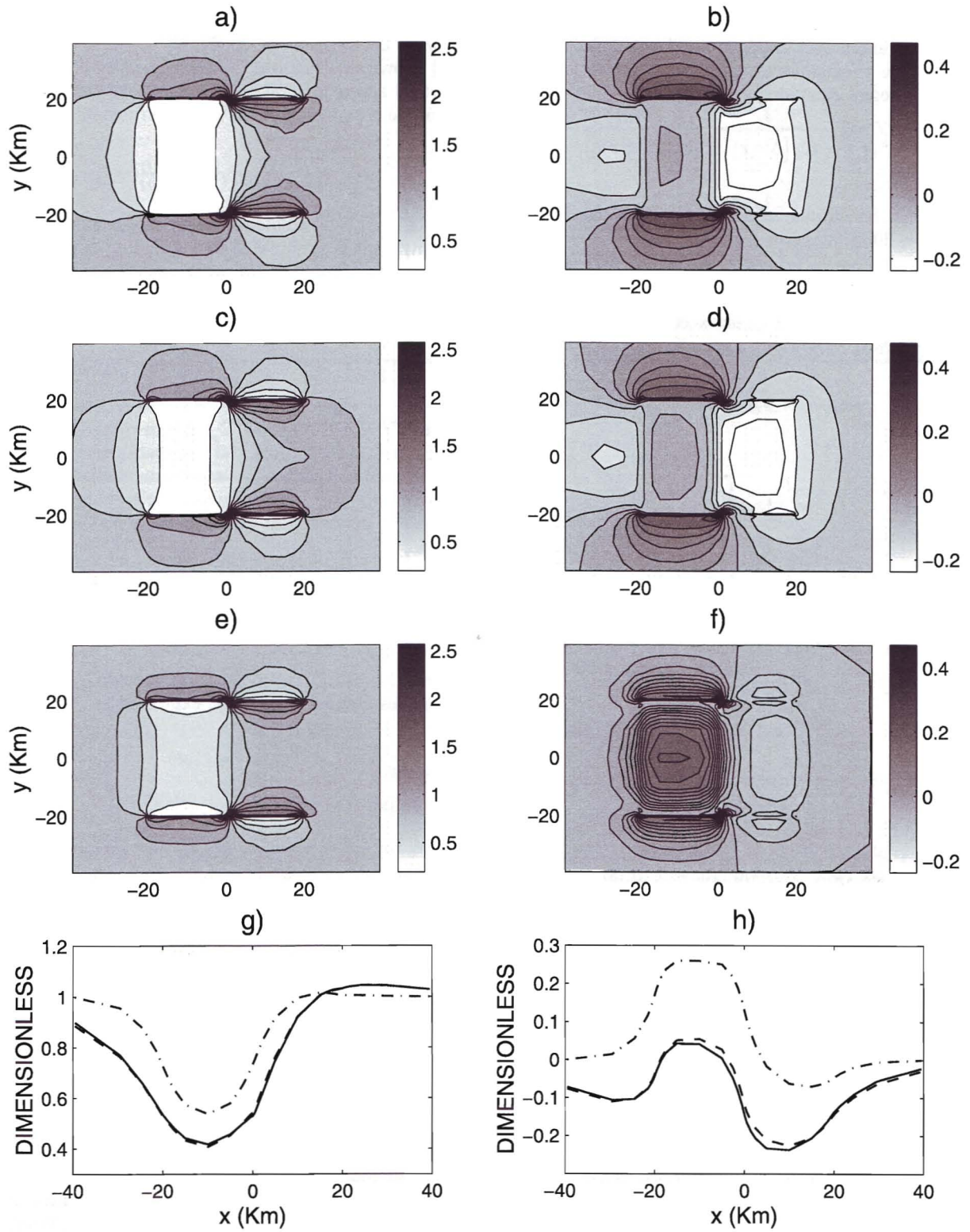
a)

b)

c)

d)

e)

f)

g)

h)

Figure 6

Table 1. Model 1[a]

| | | CPU Time, s | | |
| | | FD CPU Time | BC CPU Time | (FD + BC) CPU Time |
Method	Matrix Size			
FD with GRID-A supplemented with zero BC	156333 × 156333	3025	0	3025
FD with GRID-B supplemented with QA BC	71928 × 71928	1067	137	1204

[a]Matrix size and CPU times (in seconds) comparisons of the FD solutions obtained using GRID-A (Figure 4) with zero BC, and GRID-B (Figure 4) with QA BC.

2000]) as a boundary condition for the FD solution helps to significantly reduce the size of the modeling grid, and correspondingly the size of the matrix $(\widehat{\mathbf{D}} + i\omega\mu_0\widehat{\sigma})$ arising from equation (11). We will illustrate this point by some numerical modeling results with CPU time and matrix size reduction comparisons (Section 4).

[20] The advantages of the QA boundary conditions over traditional Dirichlet or Neumann boundary conditions with boundary values equal to zero are obvious. The QA approximation/series provides an accurate estimation of the true boundary value of the field. As a result, it is not necessary to move the boundaries far away from the inhomogeneous domain, which may be the actual modeling area of interest. At the same time the computation of the QA boundary values is a relatively simple numerical operation because it does not require a solution of any system of equations. Note also that the accuracy of the QA approximation can be increased, if necessary, by using just a few first terms of the QA series.

4. Numerical Modeling Results

[21] In this section we examine the effectiveness of the developed FD algorithm and the new QA-based boundary conditions (BC) on typical 3-D models with high resistivity contrast. In order to examine the accuracy of numerical modeling, we make a comparison between the modeling results obtained by our FD code and the full

integral equation (IE) code of *Xiong* [1992]. The electric field results to be shown are total electric field normalized by the corresponding incident normal (background) field computed at Earth's surface ($z = 0$). These calculations were performed on a 1.8 GHz PC.

4.1. Model 1

[22] This model is 3D COMMEMI model 2 [*Zhdanov et al.*, 1997]. It consists of two anomalous bodies adjacent in the y direction. The first body has a resistivity of 1 Ohm-m and dimensions of $20 \times 40 \times 10$ km in the x, y, and z directions, respectively. The second body has a resistivity of 100 Ohm-m, and the same dimensions as the first body. The normal (background) section of this model consists of three layers with resistivities, from top to bottom, of 10, 100, and 0.1 Ohm-m, respectively. The first and second layers have thicknesses of 10 and 20 km, respectively (Figure 2). The model is excited by a plane wave of 0.01 Hz frequency and an incident electric field oriented in the y direction (E_y^b polarization). The domain is discretized in the x, y, and z directions into $42 \times 32 \times 42$ cells (including 10 layers in the air extending to 75 km above Earth's surface), respectively. This discretization was supplemented with zero BC and resulted in a linear system of equations with a matrix size of 156333 × 156333, which was solved iteratively using the preconditioned generalized minimal residual (GMRES) method [*Saad and Schultz*, 1986; *Zhdanov*, 2002] (see Appendix A). Iterations were performed until the L_2 norm of the relative residuals dropped below 10^{-5}.

[23] Figures 3a and 3b show the maps of the real and imaginary parts of the E_x component at Earth's surface computed using the FD method. The corresponding responses computed using the IE method [*Xiong*, 1992] are shown in Figures 3c and 3d. Figures 3e and 3f, respectively, show comparisons of the real and imaginary parts of the E_x component computed at Earth's surface by FD and IE methods for a profile taken in the x direction.

[24] The FD grid described above (GRID-A in Figure 4) was truncated in both earth and air and produced the new grid, labeled GRID-B (Figure 4). The truncated GRID-B has a discretization of $38 \times 28 \times 25$ cells (including 6 air layers) in the x, y, and z directions, respectively, with air layers extending to 5 km above Earth's surface. Note that the size of the

Figure 6. Model 1. Electric field E_y component at Earth's surface obtained by FD modeling using different grid sizes and boundary conditions: (a and b) real and imaginary parts obtained from untruncated grid supplemented with zero BC (shown in solid line in Figures 6g and 6h); (c and d) real and imaginary parts obtained from truncated grid supplemented with QA BC (shown in dashed line in Figures 6g and 6h); (e and f) real and imaginary parts obtained from truncated grid supplemented with zero BC (shown in dash-dot line in Figures 6g and 6h); (g and h) profiles in the x direction at y = 0 km of the real and imaginary parts. The electric field results shown are total electric field normalized by the corresponding incident normal (background) field computed at Earth's surface.
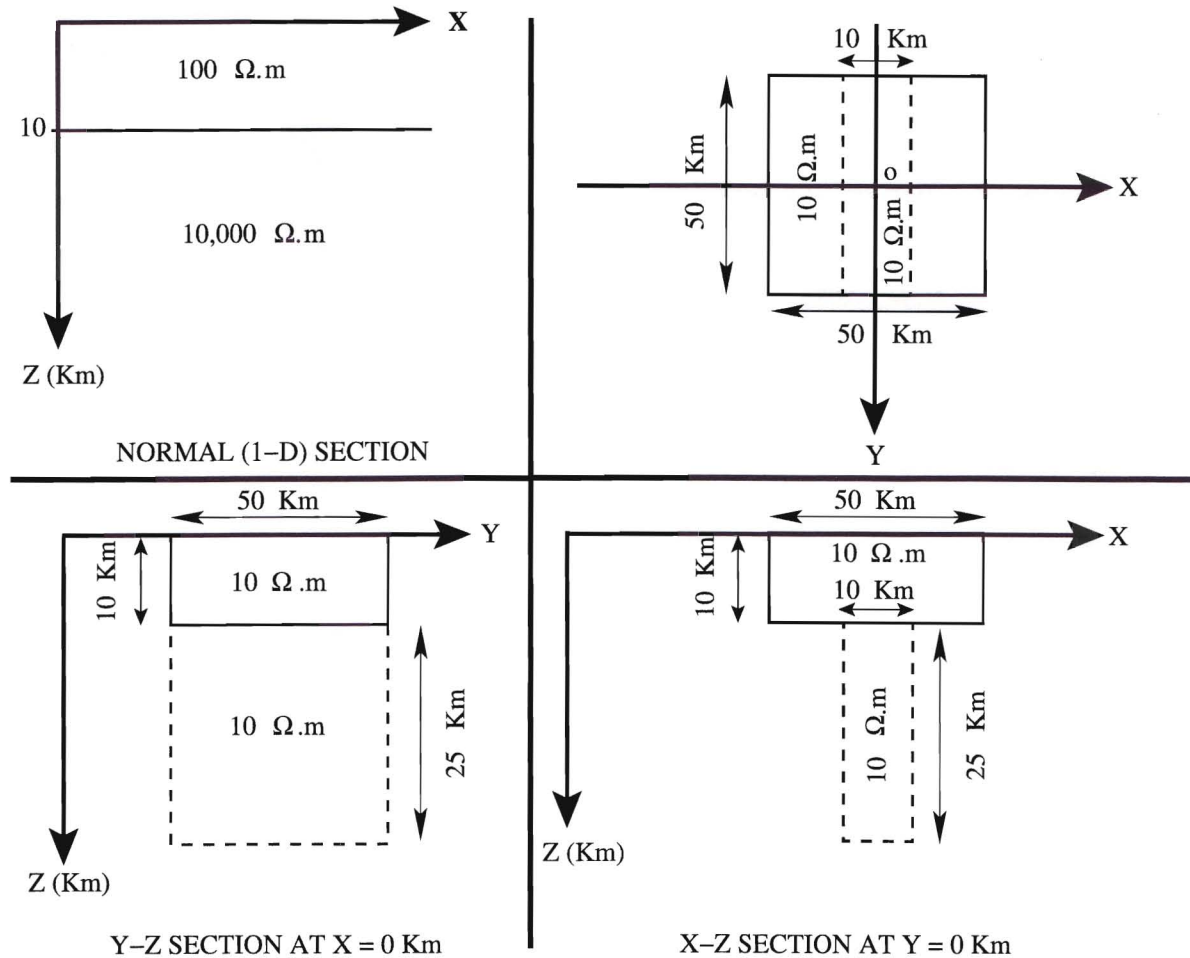
Figure 7. Model 2.

truncated grid is determined by the structure of the model. The FD algorithm for the anomalous field requires that the truncated grid (GRID-B) include the entire anomalous domain. This GRID-B was supplemented with QA BC, and its discretization resulted in a 71928×71928 linear system of equations which was solved using the same solver and accuracy mentioned above.

[25] Figures 5a, 5c, and 5e present a comparison of the real part of the E_x component computed at Earth's surface, respectively, using GRID-A with zero BC (shown as a solid line in Figure 5g), GRID-B with QA BC (shown in dashed line in Figure 5g), and GRID-B with zero BC (shown as a dash-dot line in Figure 5g). The corresponding profiles of the computed data (taken in the x direction) are shown in Figure 5g. The comparison of the imaginary part of the E_x component at Earth's surface is shown in Figures 5b, 5d, 5f, and 5h. Figure 6 presents the corresponding comparisons for the E_y component. These comparisons demonstrate that the QA BC successfully results in an accurate FD solution without demanding many discretizations from the anomalous domain.

[26] Table 1 shows the corresponding matrix size and CPU time of the FD solutions obtained using GRID-A with zero BC and GRID-B with QA BC. Column 2 of this table compares the matrix size of each method. One can clearly see that the proposed FD method with QA BC leads to a 4.7 reduction in matrix size. Columns 3, 4 and 5 present a comparison of the FD, BC and total (FD + BC) CPU times in seconds for both FD solutions. This CPU time comparison shows that the proposed method is 2.5 times faster than the FD method with zero BC.

4.2. Model 2

[27] This model consists of two anomalous bodies with a resistivity of 10 Ohm-m. The two bodies have
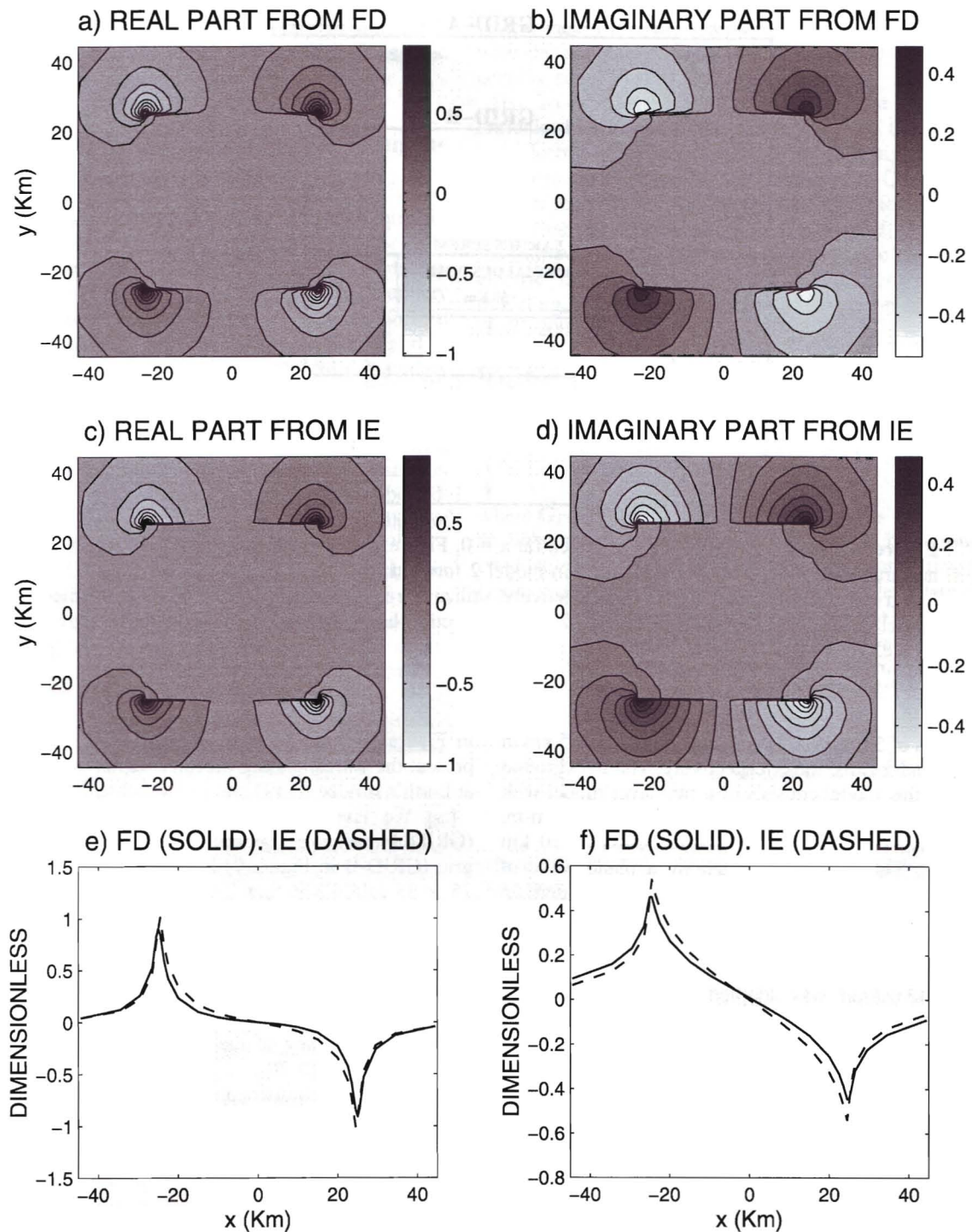
Figure 8. Model 2. Electric field E_y component at Earth's surface obtained by FD modeling and IE modeling: (a and b) real and imaginary parts obtained from FD; (c and d) real and imaginary parts obtained from IE; (e and f) profiles in the x direction at y = −25.5 km of the real and imaginary parts obtained from FD (solid) and IE (dashed). The electric field results shown are total electric field normalized by the corresponding normal (background) field computed at Earth's surface.
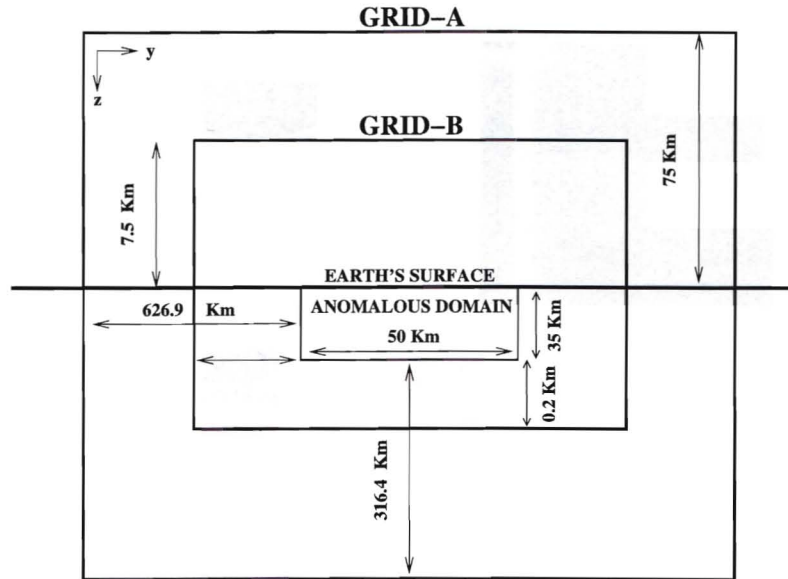
Figure 9. This figure shows a y-z sketch (at x = 0, Figure 7) of both the untruncated (GRID-A) and truncated (GRID-B) FD grids used in model 2 forward modelings in order to verify the QA-based BC. GRID-A and GRID-B, respectively, utilize the zero and QA-based BC. The detailed model description is shown in Figure 7. The x-z section has distances identical to those shown above.

dimensions of 50 × 50 × 10 km, and 10 × 50 × 25 km in the x, y, and z directions, respectively. The background section of this model consists of a two-layer model with resistivities from top to bottom of 100 and 10,000 Ohm-m, respectively. The first layer has a thickness of 10 km (Figure 7). The model is excited by a plane wave of E_x^b polarization and a frequency of 0.1 Hz. The domain is discretized in the x, y, and z directions into 50 × 35 × 44 cells (including 10 layers in air), respectively, with air layers extending to 75 km above Earth's surface. This discretization was supplemented with zero BC, and resulted in a 214914 × 214914 linear system which was solved using the same solver and accuracy above.

[28] Figures 8a and 8b show the maps of the real and imaginary parts of the E_y component at Earth's surface obtained from FD. The corresponding IE [*Xiong*, 1992] responses at Earth's surface are shown

in Figures 8c and 8d. Figures 8e and 8f, respectively, present the corresponding profile comparisons computed at Earth's surface by FD and in the x direction.

[29] We have truncated the FD grid described above (GRID-A in Figure 9) in both earth and air. The reduced grid (GRID-B in Figure 9) has a discretization of 40 × 25 × 35 cells (including 7 layers in air) in the x, y, and z directions, respectively, with air layers extending to 7.5 km above Earth's surface. This FD reduced grid was supplemented with QA BC, and its corresponding discretization resulted in a 95472 × 95472 linear system of equations which was relaxed using same solver and accuracy of the FD solution obtained from GRID-A with zero BC.

[30] The map comparisons for the real part of the E_x component computed at Earth's surface using GRID-A with zero BC (shown as a solid line in Figure 10g), GRID-B with QA BC (shown as a dashed line in

Figure 10. Model 2. Electric field E_x component at Earth's surface obtained by FD modeling using different grid sizes and boundary conditions: (a and b) real and imaginary parts obtained from untruncated grid supplemented with zero BC (shown in solid line in Figures 10g and 10h); (c and d) real and imaginary parts obtained from truncated grid supplemented with QA-based BC (shown in dashed line in Figures 10g and 10h); (e and f) real and imaginary parts obtained from truncated grid supplemented with zero BC (shown in dash-dot line in Figures 10g and 10h); (g and h) profiles in the x direction at y = 0 km of the real and imaginary parts. The electric field results shown are total electric field normalized by the corresponding incident normal (background) field computed at Earth's surface.
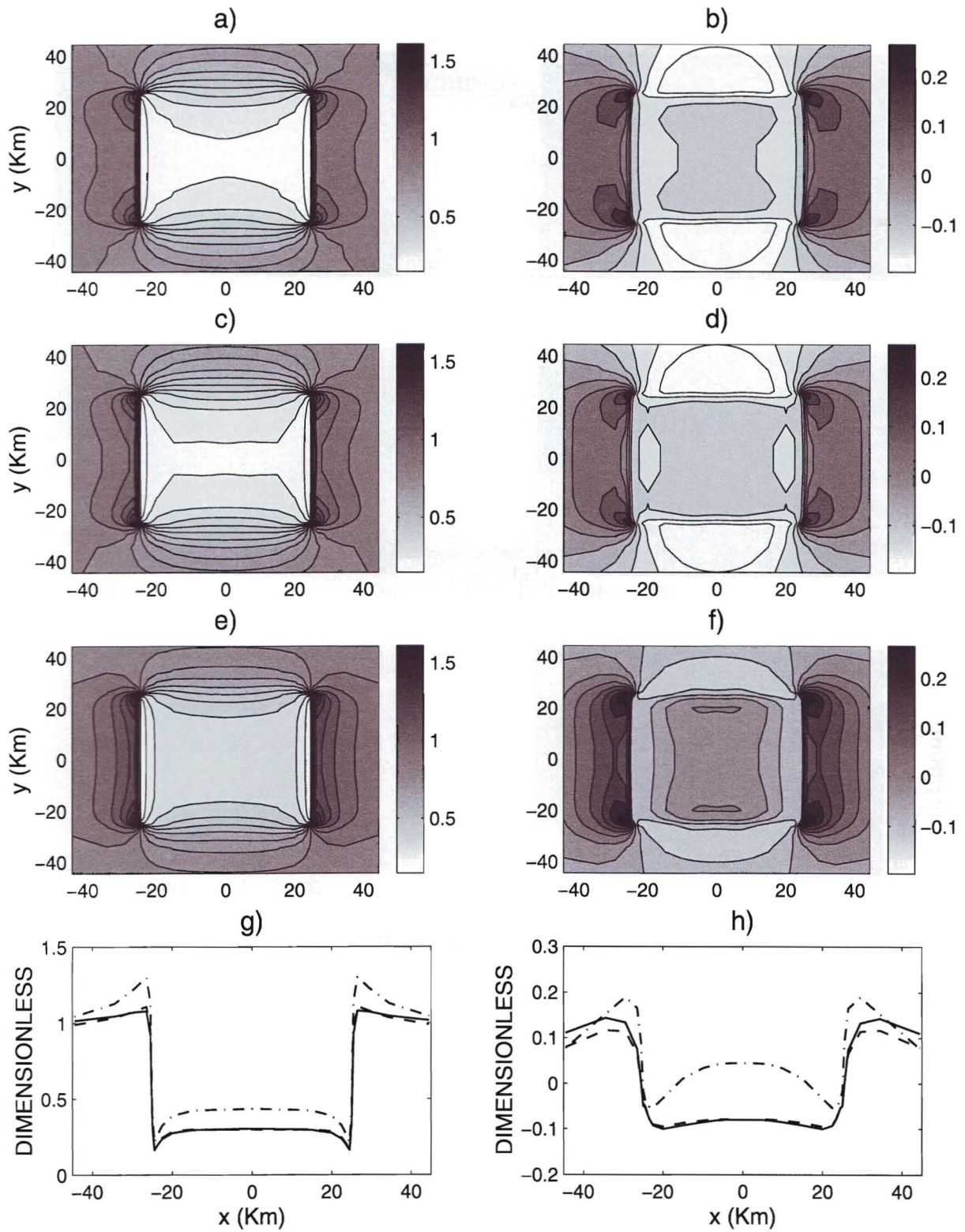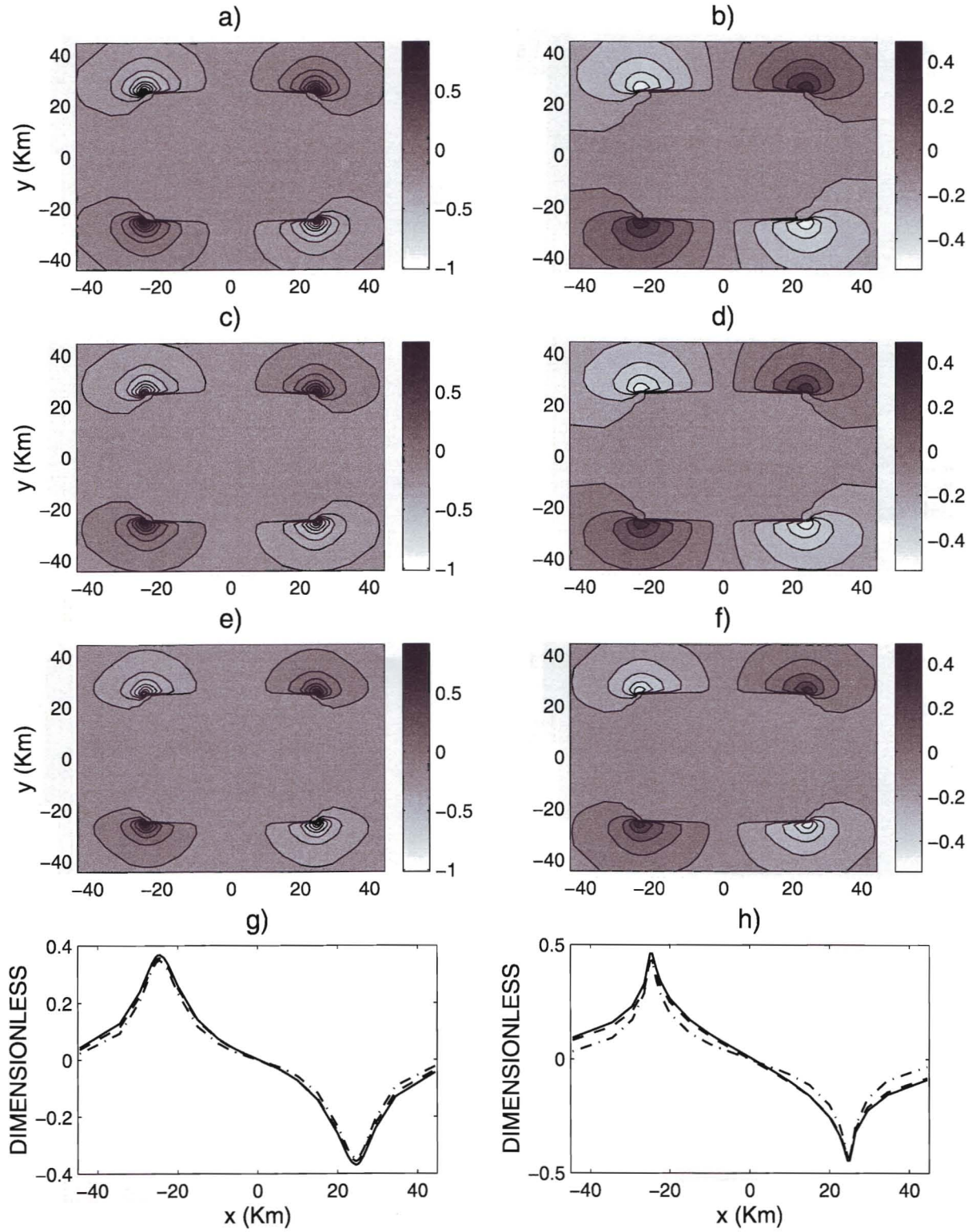
Figure 10

Figure 11

Table 2. Model 2[a]

		CPU Time, s		
Method	Matrix Size	FD CPU Time	BC CPU Time	(FD + BC) CPU Time
FD with GRID-A supplemented with zero BC	214914 × 214914	4647	0	4647
FD with GRID-B supplemented with QA BC	95472 × 95472	1645	226	1871

[a]Matrix size and CPU times (in seconds) comparisons of the FD solutions obtained using GRID-A (Figure 20) with zero BC, and GRID-B (Figure 20) with QA BC.

Figure 10g), and GRID-B with zero BC (shown in dash-dot line in Figure 10g) are shown in Figures 10a, 10c, and 10e, respectively. The corresponding profile comparisons made in the x direction are shown in Figure 10g. The imaginary part comparisons of the E_x component computed at Earth's surface are shown in Figures 10b, 10d, 10f, and 10h. Figure 11 presents the corresponding comparisons of the real and imaginary parts of the E_y component at Earth's surface.

[31] Table 2 shows a comparison of the corresponding matrix size and CPU time of the FD solutions obtained using GRID-A with zero BC and GRID-B with QA BC. Column 2 of this table presents the matrix size of each method. One can see that the proposed FD method with QA BC leads to a five times reduction in matrix size. A comparison of the FD, BC and total (FD + BC) CPU times in seconds for both FD solutions is presented in columns 3, 4 and 5. This CPU time comparison shows that the proposed method is about 2.5 times faster than the FD method with zero BC.

5. Conclusions

[32] In this paper we have presented a new approach for three-dimensional finite difference electromagnetic modeling in the frequency domain based on the balance method and the quasi-analytical boundary condition for truncation of the modeling area. This approach helps reduce the size of the modeling grid significantly without losing the accuracy of calculation. As a result, a larger number of fine grid cells can be used to describe the anomalous conductivity distribution within the modeling domain.

Appendix A: Solution of the Linear System of Finite Difference Equations

[33] The resulting system of linear algebraic FD equations and the accompanying boundary conditions (11) can be expressed in matrix notation as:

$$\widehat{\mathbf{A}}\mathbf{e}^a = \mathbf{b}, \tag{A1}$$

where $\widehat{\mathbf{A}} = \widehat{\mathbf{D}} + i\omega\mu_0\widehat{\sigma}$, and equation (A1) is a $3N \times 3N$ linear system with respect to the anomalous electric field. We solve this system using the Generalized Minimal Residual (GMRES) method. The basic idea of the GMRES method [Saad and Schultz, 1986; Zhdanov, 2002] is to find the solution along an orthonormal basis:

$$\left\{\widehat{\mathbf{A}}\mathbf{g}_1^n, \widehat{\mathbf{A}}\mathbf{g}_2^n, \cdots, \widehat{\mathbf{A}}\mathbf{g}_s^n\right\}$$

in the Krylov subspace

$$\mathcal{K} = span\left\{\widehat{\mathbf{A}}\mathbf{r}_n, \widehat{\mathbf{A}}^2\mathbf{r}_n, \cdots, \widehat{\mathbf{A}}^k\mathbf{r}_n\right\}.$$

At the n-th step of the iterative process

$$\mathbf{x}_{n+1} = \mathbf{x}_n - \sum_{l=1}^{s} k_{nl}\mathbf{g}_l^{(n)}, \; s \leq n,$$

where $\mathbf{r}_n = \widehat{\mathbf{A}}\mathbf{x}_n - \mathbf{b}$. The more orthonormal basis functions are calculated (the larger s is), the smoother the convergence becomes, requiring a fewer number of iterations with smaller amplification of the roundoff errors during the iterative process. However, at each iteration, the orthogonalization process performed requires $2s$ matrix multiplications, and the number of vectors to be stored is also proportional to s. The convergence rate of the GMRES iterative algorithm can be increased dramatically by using the corresponding preconditioners [Golub and Van Loan, 1996].

Figure 11. Model 2. Electric field E_y component at Earth's surface obtained by FD modeling using different grid sizes and boundary conditions: (a and b) real and imaginary parts obtained from untruncated grid supplemented with zero BC (shown in solid line in Figures 11g and 11h); (c and d) real and imaginary parts obtained from truncated grid supplemented with QA-based BC (shown in dashed line in Figures 11g and 11h); (e and f) real and imaginary parts obtained from truncated grid supplemented with zero BC (shown in dash-dot line in Figures 11g and 11h); (g and h) profiles in the x direction at y = −29.5 km of the real and imaginary parts. The electric field results shown are total electric field normalized by the corresponding incident normal (background) field computed at Earth's surface.

References

Anderson, W. L. (1979), Numerical integration of related Hankel transforms of orders 0 and 1 by adaptive digital filtering, *Geophysics, 44*, 1287.

Balay, S., W. D. Gropp, L. C. McInnes, and B. F. Smith (1997), Efficient management of parallelism in object oriented numerical software libraries, in *Modern Software Tools in Scientific Computing*, edited by E. Arge, A. M. Bruaset, and H. P. Langtangen, Birkhäuser Boston, Cambridge, Mass.

Balay, S., W. D. Gropp, L. C. McInnes, and B. F. Smith (2000), PETSc 2.0 users manual (ANL-95/11—Revision 2.0.28), Argonne Natl. Lab., Chicago, Ill.

Berdichevsky, M. N., and M. S. Zhdanov (1984), *Advanced Theory of Deep Geomagnetic Sounding*, Elsevier Sci., New York.

Berenger, J. P. (1994), A perfectly matched layer for the absorption of the electromagnetic waves, *J. Comput. Phys., 114*, 185.

Davydycheva, S., V. Druskin, and T. Habashy (2003), An efficient finite-difference scheme for electromagnetic logging in 3D anisotropic inhomogeneous media, *Geophysics, 68*, 1525.

Fomenko, E., and T. Mogi (2002), A new computation method for a staggered grid of 3D EM field conservative modeling, *Earth Planets Space, 54*, 499.

Golub, G. H., and C. F. Van Loan (1996), *Matrix Computation*, 3rd ed., Johns Hopkins Univ. Press, Baltimore, Md.

Habashy, T. M., R. W. Groom, and B. R. Spies (1993), Beyond the Born and Rytov approximations: A nonlinear approach to electromagnetic scattering, *J. Geophys. Res., 98*, 1759.

Haber, E., U. M. Ascher, D. A. Aruliah, and D. W. Oldenburg (2000), Fast simulation of 3D electromagnetic problems using potentials, *J. Comput. Phys., 163*, 150.

Hursan, G., and M. S. Zhdanov (2002), Contraction integral equation method in three-dimensional electromagnetic modeling, *Radio Sci., 37*(6), 1089, doi:10.1029/2001RS002513.

Kincaid, D., and W. Cheney (1996), *Numerical Analysis*, 2nd ed., Brooks/Cole Publ. Co., Pacific Grove, Calif.

Mackie, R. L., T. R. Madden, and P. E. Wannamaker (1993), Three-dimensional magnetotelluric modeling using difference equations—Theory and comparisons to integral equation solutions, *Geophysics, 58*, 215.

Mackie, R. L., J. T. Smith, and T. R. Madden (1994), Three-dimensional electromagnetic modeling using finite difference equations: The magnetotelluric example, *Radio Sci., 29*, 923.

Mehanee, S. (2003), Multidimensional finite difference electromagnetic modeling and inversion based on the balance method, Ph.D. thesis, Univ. of Utah, Salt Lake City.

Mehanee, S., and M. Zhdanov (2001), 3-D finite-difference forward modeling based on the balance method, in *71st Ann. Internat. Mtg. Soc. Expl. Geophys., Expanded Abstracts*, p. 1443, Soc. of Explor. Geophys., Tulsa, Okla.

Morse, P. M., and H. Feshbach (1953), *Methods of Mathematical Physics, Part 1*, McGraw-Hill, New York.

Newman, G., and D. Alumbaugh (1995), Frequency-domain modelling of airborne electromagnetic responses using staggered finite differences, *Geophys. Pros., 43*, 1021.

Saad, Y., and M. N. Schultz (1986), GMRES: A generalized minimal residual algorithm for solving a nonsymmetric linear system, *SIAM J. Sci. Stat. Comput., 7*, 856.

Samarsky, A. (1984), *Theory of the Difference Schemes* (in Russian), Nauka, Moscow.

Smith, J. T. (1996), Conservative modeling of 3-D electromagnetic fields; part II: Bi-conjugate gradient solution and an accelerator, *Geophysics, 61*, 1319.

Spichak, V. (1999), *Magnetotelluric Fields in Three-Dimensional Geoelectrical Models* (in Russian), Sci. World, Moscow.

Turkel, E., and A. Yefet (1998), Absorbing PML boundary layers for wave-like equations, *Appl. Numer. Math., 27*, 533.

Wang, T., and G. W. Hohmann (1993), A finite difference time-domain solution for three dimensional electromagnetic modeling, *Geophysics, 58*, 797.

Wang, T., and S. Fang (2001), 3-D electromagnetic anisotropy modeling using finite differences, *Geophysics, 66*, 1386.

Wannamaker, P. E., G. W. Hohmann, and W. A. SanFilipo (1984), Electromagnetic modeling of three dimensional bodies in layered earths using integral equations, *Geophysics, 49*, 60.

Weaver, J. T. (1994), *Mathematical Methods for Geo-Electromagnetic Induction*, Res. Stud. Press, Taunton, Mass.

Weaver, J. T., and C. R. Brewitt-Taylor (1978), Improved boundary conditions for the numerical solution of E-polarization problems in geomagnetic induction, *Geophys. J. R. Astron. Soc., 87*, 917.

Xiong, Z. (1992), EM modeling of three-dimensional structures by the method of system iteration using integral equations, *Geophysics, 57*, 1556.

Yee, K. S. (1966), Numerical solution of initial boundary problems involving Maxwell's equations in isotropic media, *IEEE Trans. Antennas Propag., 14*, 302.

Zhdanov, M. S. (1988), *Integral Transforms in Geophysics*, Springer-Verlag, New York.

Zhdanov, M. S. (2002), *Geophysical Inverse Theory and Regularization Problems*, Elsevier Sci., New York.

Zhdanov, M. S., and G. V. Keller (1994), *The Geoelectrical Methods in Geophysical Exploration*, Elsevier Sci., New York.

Zhdanov, M. S., and V. V. Spichak (1989), Mathematical modeling of three-dimensional quasi-stationary electromagnetic fields in geoelectrics (in Russian), *Dokl. Akad. Nauk. SSSR*, *309*, 57.

Zhdanov, M. S., and V. V. Spichak (1992), *Mathematical Modeling of Electromagnetic Fields in Three-Dimensional Inhomogeneous Media*, (in Russian), Nauka, Moscow.

Zhdanov, M. S., N. G. Golubev, V. V. Spichak, and I. M. Varentsov (1982), The construction of effective methods for electromagnetic modeling, *Geophys. J. R. Astron. Soc.*, *68*, 589.

Zhdanov, M. S., I. M. Varentsov, J. T. Weaver, N. G. Golubev, and V. A. Krylov (1997), Methods for modeling electromagnetic fields. Results from COMMEMI—The international project on the comparison of modeling methods for electromagnetic induction, *J. Appl. Geophys.*, *37*, 1.

Zhdanov, M. S., V. I. Dmitriev, S. Fang, and G. Hursan (2000), Quasi-analytical approximations and series in electromagnetic modeling, *Geophysics*, *65*, 1746.

S. Mehanee, Department of Geology and Geophysics, University of Utah, 135 South 1460 East, Room 719, Salt Lake City, UT 84112, USA.

M. S. Zhdanov, Consortium for Electromagnetic Modeling and Inversion, Department of Geology and Geophysics, University of Utah, Salt Lake City, UT 84112-0111, USA. (mzhdanov@mines.utah.edu)